Detection and Estimation of Unmodeled Chirps

Soumya D. Mohanty
Department of Physics and Astronomy
The University of Texas Rio Grande Valley
One West University Blvd
Brownsville, TX 78520, USA
Email: soumya.mohanty@utrgv.edu

***Abstract*—The detection and estimation of transient chirp signals with unmodeled amplitude envelope and instantaneous frequency evolution is a significant challenge in gravitational wave (GW) data analysis. We review a recently introduced method that addresses this challenge using a spline-based approach. The applicability of this method to the important problem of removing non-transient chirps in GW data, namely narrowband noise of instrumental and terrestrial origin, is investigated.**

I. Introduction

The decades long effort to open the gravitational wave (GW) window in astronomy has now been realized by the LIGO [1] and Virgo [2] detectors. The GW signals detected so far [3] have waveforms that can be calculated theoretically, allowing matched filtering [4] to be used for their detection and estimation. This approach is inapplicable, however, to GW signals from astrophysical sources that are unanticipated or that are difficult to model theoretically. Among such unmodeled signals – known as GW bursts when they are transient – the case of chirps is particularly challenging.

Taking the analytic representation, $a(t)\exp(i\phi(t))$, of a signal $s(t)$, one can operationally define $s(t)$ to be a chirp when the amplitude envelope $a(t)$ and instantaneous frequency $f(t) = \dot{\phi}(t)$ evolve adiabatically – $f(t) \gg \dot{a}/a$ and $f^2(t) \gg \dot{f}(t)$ – relative to the instantaneous period $1/f(t)$.

The author has recently proposed a new method [5], called Spline Enabled Effectively-Chirp Regression (SEECR), to address the detection and estimation of unmodeled transient chirps. A direct comparison with a method based on multi-resolution time-frequency clustering, which is the paradigm underyling current burst search methods in LIGO [6]–[9], shows that SEECR has a significantly better performance.

While the focus in the case of GW chirps has mainly been on transient signals, it is interesting to note that real data from GW detectors is actually full of very strong non-transient chirps! These are the myriad narrowband interferences, called line noise, contaminating the data that arise from diverse sources such as the power supply (at 60 Hz and harmonics in the United States) and mechanical resonances. As shown in Fig. 1, these lines are usually very strong, rising several tens of dB above the nominal broadband noise floor, and all GW search methods need to employ some data conditioning step to mitigate them before any kind of analysis can begin.

In this paper, we provide a condensed review of SEECR and its performance on transient chirps, followed by a first investigation of its use in removing lines. The reader can find a more extensive description of SEECR, and a statistically rigorous characterization of its performance on transient chirps, in [5]. The results presented here are largely independent of those in [5] and complementary.

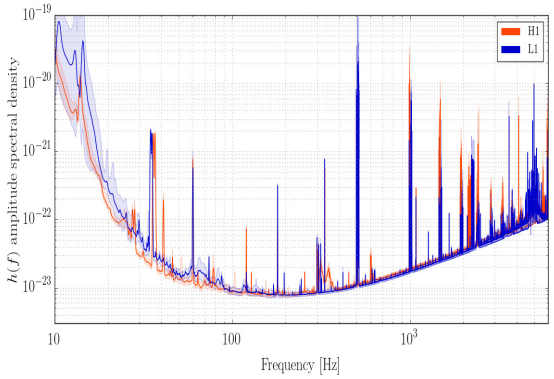

Fig. 1. The estimated sensitivity curve – defined as the square root of the noise Power Spectral Density – for the LIGO detector at Hanford (red) and Livingston (blue) showing high power narrowband (line) features. (Image credit: LIGO Open Science Center.)

II. Description of the Method

The essential idea behind SEECR is to make no assumptions about $a(t)$ and $f(t)$ except that they are smooth. This requirement is implemented by representing them as mutually independent splines. Fig. 2 shows a schematic illustration of how this model is constructed. The signal model is estimated from the data using a penalized spline fitting procedure. The splines have continuously adjustable breakpoints that are optimized [10] using Particle Swarm Optimization (PSO) [11]. Finally, model selection is used to choose the best number of breakpoints for the splines.

Notation: $\overline{s} \in \mathbb{R}^N$ denotes a row vector with N elements, and s_j, $j = 0, 1, \ldots, N-1$, or $[\overline{s}]_j$, denotes its j^{th} element. Where $\overline{s}$ is a sequence of discrete-time samples of $s(t)$, the sampling times are denoted by t_i, $i = 0, 1, \ldots, N-1$, and $s_i = s(t_i)$. $\mathbf{A}$ denotes a matrix with the element in its i^{th} row and j^{th} column denoted by A_{ij} or $[\mathbf{A}]_{ij}$. The identity matrix is denoted by $\mathbf{I}$.

ISBN 978-90-827970-1-5 © EURASIP 2018

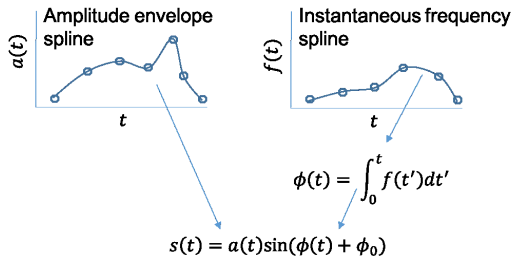

Fig. 2. A schematic of the signal model used in SEECR. Open circles denote the data points interpolated by a spline, their respective time coordinates being the set of breakpoints asssociated with the spline. (ϕ_0 denotes the initial phase of the signal.)

A. Data Model

Let $\overline{y}$ denote a segment of GW detector output, sampled uniformly with a sampling frequency f_s. Under the null and alternative hypotheses, denoted by H_0 and H_1 respectively,

$$\overline{y} \;=\; \begin{cases} \overline{n} & ; H_0 \\ \overline{s}+\overline{n} & ; H_1 \end{cases} , \tag{1}$$

where $\overline{s}$ is a GW signal and $\overline{n}$ is a realization of noise. Without loss of generalization, the noise $\overline{n}$ can be assumed to be drawn from a zero mean, unit variance iid Normal process (i.e., white noise) with $E[n_i n_j] = \delta_{ij}$.

Let $a(t;\overline{\alpha},\overline{\tau}_a)$ denote the spline for $a(t)$, where $\overline{\tau}_a \in \mathbb{R}^M$ are the breakpoints,

$$a(t;\overline{\alpha},\overline{\tau}_a) \;=\; \sum_{j=0}^{M-1} \alpha_j \mathcal{B}_{j,k}(t;\overline{\tau}_a) , \tag{2}$$

and $\mathcal{B}_{j,k}(t;\overline{\tau}_a)$ is a B-spline function [12] of order k. Since B-splines have compact support, $a(t;\overline{\alpha},\overline{\tau}_a) = 0$ for $t \notin [\tau_{a,0}, \tau_{a,M-1}]$, where $\tau_{a,i} = [\overline{\tau}_a]_i$.

Let $f(t;\overline{\nu},\overline{\tau}_f)$ be the spline corresponding to $f(t)$, where $\overline{\tau}_f \in \mathbb{R}^K$ and $\overline{\nu} \in \mathbb{R}^K$ denote the breakpoints and corresponding instantaneous frequencies that the spline must interpolate.

With $\overline{\nu}$, $\overline{\tau}_a$, and $\overline{\tau}_f$ denoted collectively by $\overline{\theta}$, the signal model is given by,

$$s(t_i;\overline{\alpha},\overline{\theta},\phi_0) \;=\; a(t_i;\overline{\alpha},\overline{\tau}_a)\sin(\phi(t_i;\overline{\nu},\overline{\tau}_f)+\phi_0) , \tag{3}$$

$$\phi(t;\overline{\nu},\overline{\tau}_f) \;=\; \begin{cases} 0, & t < \tau_{a,0} \\ \int_{\tau_{a,0}}^{t} dt' f(t';\overline{\nu},\overline{\tau}_f), & t \le \tau_{a,M-1} \end{cases} \tag{4}$$

Let $\mathbf{X}_0$ and $\mathbf{X}_1$ denote matrices given by

$$[\mathbf{X}_1(\overline{\theta}) + i\mathbf{X}_0(\overline{\theta})]_{j,m} \;=\; \mathcal{B}_{j,k}(t_m;(\overline{\tau}_a)e^{i\phi(t_m;\overline{\nu},\overline{\tau}_f)} . \tag{5}$$

In terms of these matrices, the signal sequence is,

$$\overline{s}(\overline{\alpha},\overline{\theta},\phi_0) \;=\; \overline{\beta}\mathbf{X}(\overline{\theta}) , \tag{6}$$

$$\overline{\beta} \;=\; \overline{\alpha}\mathbf{\Phi}_0 ,$$

$$\mathbf{\Phi}_0 \;=\; \begin{pmatrix} \cos\phi_0\mathbf{I} & \sin\phi_0\mathbf{I} \end{pmatrix} , \tag{7}$$

$$\mathbf{X}(\overline{\theta}) \;=\; \begin{pmatrix} \mathbf{X}_0(\overline{\theta}) \\ \mathbf{X}_1(\overline{\theta}) \end{pmatrix} . \tag{8}$$

B. Model estimation

The signal model in (6) is estimated by minimizing

$$\Lambda(\overline{\alpha},\overline{\theta},\phi_0|\overline{y},\lambda) \;=\; R(\overline{\alpha},\overline{\theta},\phi_0|\overline{y}) + \lambda\overline{\alpha}\,\overline{\alpha}^T , \tag{9}$$

$$R(\overline{\alpha},\overline{\theta},\phi_0|\overline{y}) \;=\; \|\overline{y} - \overline{s}(\overline{\alpha},\overline{\theta},\phi_0)\|^2 , \tag{10}$$

with $\|\overline{x}\|$ being the L_2 norm of $\overline{x}$, over $\overline{\alpha}$, $\overline{\theta}$, and ϕ_0 using the following program of nested minimizations,

$$\min_{\overline{\alpha},\overline{\theta},\phi_0} \Lambda \;=\; \min_{\overline{\theta}} \left(\min_{\phi_0} \left(\min_{\overline{\alpha}} \Lambda \right) \right) . \tag{11}$$

The innermost minimization corresponds to the penalized spline method [13]. Henceforth, we drop the explicit listing of parameters wherever it aids clarity.

The positivity of the amplitude envelope, $a(t) \ge 0$, and B-splines, $\mathcal{B}_{j,k}(t;\overline{\tau}_a) \ge 0$, $\forall t$, requires that the innermost minimization be performed under a positivity constraint $\alpha_i \ge 0$, $\forall i$. For this task, we use the mixed primal-dual bases algorithm developed by Fraser and Massam [14].

The regulator gain, λ, is determined by minimizing the Generalized Cross-Validation (GCV) function [15]. This is merged into the minimization program at the second step as follows.

$$\lambda_{\mathrm{GCV}} \;=\; \arg\min_{\lambda} \mathrm{GCV}(\lambda;\phi_0(\lambda)) , \tag{12}$$

$$\phi_0(\lambda) \;=\; \arg\min_{\phi_0} \Lambda(\widehat{\alpha}_{\lambda,\phi_0},\overline{\theta},\phi_0|\overline{y}) , \tag{13}$$

where $\widehat{\alpha}_{\lambda,\phi_0}$ is the innermost minimizer in (11) for a given λ and ϕ_0. Both of the minimizations above are straightforward to perform numerically.

Let $\widehat{\alpha} = \widehat{\alpha}_{\lambda_{\mathrm{GCV}},\phi_0(\lambda_{\mathrm{GCV}})}$ and let the corresponding value of Λ be denoted by

$$F(\overline{\theta}|\overline{y}) \;=\; \Lambda(\widehat{\alpha},\overline{\theta},\phi_0(\lambda_{\mathrm{GCV}})|\overline{y}) , \tag{14}$$

which we call the *fitness function* in the following. The next step in the program given by (11) is the minimization of the fitness function over the parameters $\overline{\tau}_a$, $\overline{\nu}$,and $\overline{\tau}_f$.

We use PSO to tackle this high-dimensional non-convex global optimization problem after making the following simplifications. (i) The dimensionality of the search space is lowered by (a) identifying the two end breakpoints in $\overline{\tau}_a$ and $\overline{\tau}_f$, i.e., $[\overline{\tau}_f]_0 = \tau_{a,0}$ and $[\overline{\tau}_f]_{K-1} = \tau_{a,M-1}$, and (b) letting the spacing of the breakpoints in $\overline{\tau}_a$ be uniform. (ii) A reparametrization [16] of $\overline{\tau}_f$ is made to enforce monotonicity, thereby mitigating degeneracies in the fitness function.

The final step in SEECR is model selection using the Akaike Information Criterion (AIC) [17] to pick the best values of the number of breakpoints M and K in $\overline{\tau}_a$ and $\overline{\tau}_f$ respectively. The use of GCV and model selection ensures that, in most situations, the user needs to explore only a range of values for M and K in order to tune SEECR.

III. Performance on Transient Chirps

We examine the detection and estimation performance of SEECR on a set of three chirps that are widely different in

ISBN 978-90-827970-1-5 © EURASIP 2018

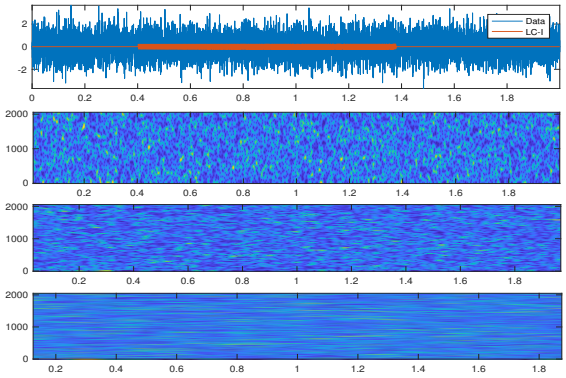

Fig. 3. The plot at the top shows the time series of a data realization (in blue) with an embedded SNR $= 10$ LC-I signal that is shown by the time series in red. The remaining plots show the spectrogram of this data realization at three different time-frequency resolutions (short segment lengths of 64, 256, and 1024 samples from top to bottom). The sampling frequency of the time series is 4096 Hz and its duration is 2.0 sec. In all the plots, the horizontal axis is time (sec). The vertical axis in each spectrogram is frequency (Hz).

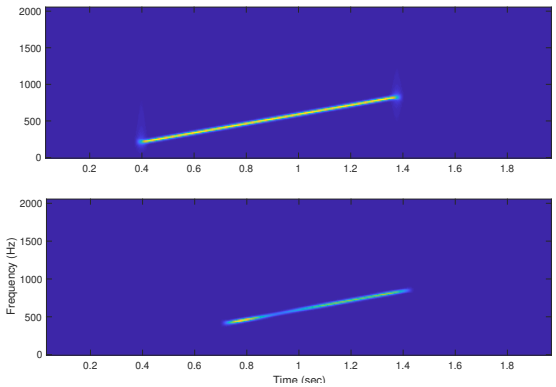

Fig. 4. The plot at the top is the spectrogram of the LC-I signal that is embedded in the data realization shown in Fig. 3. The bottom plot shows the spectrogram of the signal estimated by SEECR.

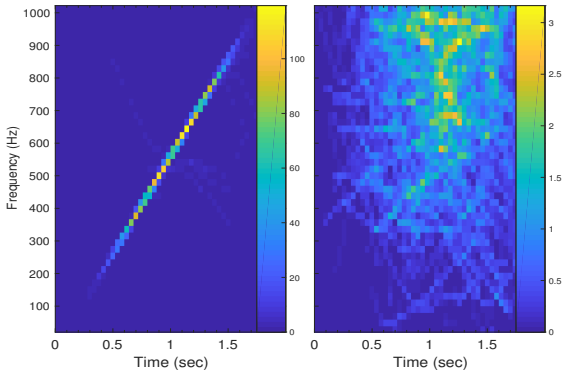

Fig. 5. Two dimensional histogram of estimated instantaneous frequencies for (left panel) data realizations containing the LC-I signal with SNR $= 10$, and (right panel) noise-only data. Each histogram is constructed by plotting all the estimated frequencies and counting the number of plotted points in a regular grid of 2D bins. There are 50 bins along each dimension. The counts in each panel are normalized by the respective number of trials used.

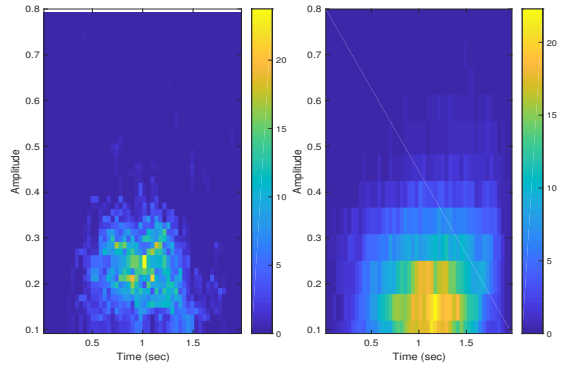

Fig. 6. Two dimensional histogram of estimated amplitude envelopes for (left panel) data realizations containing the LC-I signal with SNR $= 10$, and (right panel) noise-only data. Each histogram is constructed by plotting all the estimated amplitude envelopes and counting the number of plotted points in a regular grid of 2D bins. There are 50 bins along each dimension. The counts in each panel are normalized by the respective number of trials used.

morphology: (i) Linear Chirp with increasing frequency (LC-I), (ii) Linear Chirp with decreasing frequency (LC-D), and (iii) Quadratic Chirp (QC). In each case the signal is embedded in a simulated white noise with a matched filtering SNR – defined as the L_2 norm of the signal – of 10. The settings for the SEECR parameters are fixed in all three cases at $M \in \{5, 6, 7, 9, 11\}$ and $K \in \{3, 4, 5, 7\}$ respectively. The settings for PSO [18] are the same as used in [19], to which we refer the reader for further details. For the above set of M and K values, the dimensionality of the search space for PSO ranges between 6 and 14.

Fig. 3 shows a realization of simulated data along with its spectrograms at different time-frequency resolutions. The signal is too weak to show up clearly in any of the spectrograms, indicating that time-frequency based burst search method cannot detect this signal. Fig. 4 shows spectrograms of the LC-I signals used in Fig. 3 and the signal estimated by SEECR.

In Fig. 5, we compare the estimated instantaneous frequencies for data realizations containing the LC-I signal and noise-only data. A similar plot for the estimated amplitude envelope of the signal is shown in Fig. 6. It is clear that SEECR estimates the instantaneous frequency, even at a low SNR, quite well. As expected from the Cramer-Rao lower bound, which says that the amplitude of a monochromatic signal is always estimated with a higher error than its frequency, the error in the estimation of $a(t)$ is also higher than $f(t)$. (The estimation performance of SEECR is analyzed using quantitative metrics in [5].)

Table I lists the detection probabilities obtained for the three signals at SNR values of 10 and 12. The performance of SEECR is seen to improve rapidly with a modest rise in the SNR of these signals.

IV. Mitigating Line Noise

The line mitigation method currently used in GW burst searches is the Linear Predictive Filter (LPF) [20]. In the LPF,

ISBN 978-90-827970-1-5 © EURASIP 2018

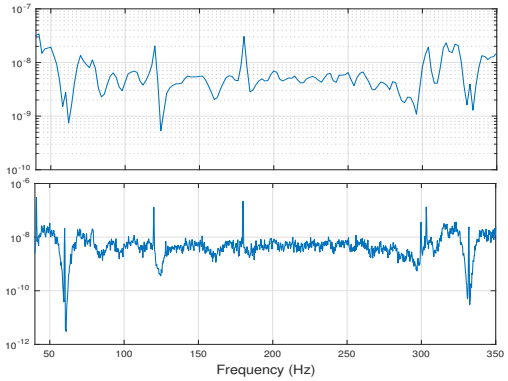

Fig. 7. PSD (arbitrary units) of the prediction error sequence produced by LPF acting on LIGO data at a frequency resolution of (top) 2 Hz, and (bottom) 0.25 Hz. The whitening in the frequency band shown is evident when compared to the sensitivity curve in Fig. 1. That LPF does notch filtering is seen clearly from the dips (note the logarithmic scale) at the power line frequency at 60 Hz (also at 332 Hz) in the finer resolution PSD (bottom). However, the notching is masked in the PSD at coarser resolution (top). The data used to produce these plots was obtained from the LIGO Open Science Center (GW150914; 32 sec of H1 data; downsampled to 1024 Hz and high pass filtered). LPF is available as the in-built function `lpc` in Matlab [22].

a predictor, $\widehat{x}[n]$, for the n^{th} sample, $x[n]$, of data is obtained as a linear combination, $\widehat{x}[n] = \sum_{j=1}^{M} c[j]x(n-j)$, of past samples. The coefficients $c[j]$, $j = 1$ to M, are trained by minimizing the variance of the prediction error $x[n] - \widehat{x}[n]$.

The Power Spectral Density (PSD) of the prediction error sequence appears white on a frequency scale $\gtrapprox f_s/M$ [21]. Hence, if a time-frequency transform based burst search method sets its frequency resolution to be coarser than the LPF whitening scale, it can analyze the prediction error sequence as effectively having white noise. However, the LPF is actually a notch filter, as seen in Fig. 7, and its output is not white for search methods such as SEECR.

Being a notch filter, the LPF is susceptible to non-stationarity in lines because it can only mitigate lines at the frequencies exhibited in the data used for training the filter coefficients. As noted in [23], imperfectly notched non-stationary lines lead to spurious transients that can mimic GW signals.

Exploiting the fact that lines are generally very high power features, it should be possible to have an alternative approach that treats lines as simply non-transient unmodeled signals and estimates them with non-parametric methods [24], [25]. Unlike the LPF output, data cleaned in this manner can function as a universal input to all GW search methods. Since SEECR is designed to estimate unmodeled chirps and operates at much

Signal	Detection Probability	
	SNR=10	SNR=12
LC-I	0.52 ± 0.07	0.90 ± 0.04
LC-D	0.48 ± 0.07	0.92 ± 0.04
QC	0.61 ± 0.04	0.97± 0.01

TABLE I

ESTIMATED DETECTION PROBABILITIES, AND THEIR 1σ ERROR INTERVALS AT A FALSE ALARM RATE OF 10^{-3} EVENTS/SEC.

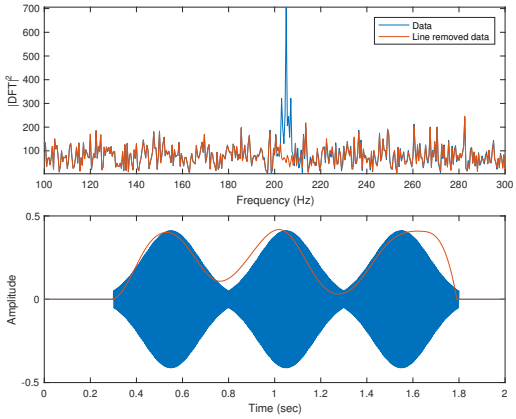

Fig. 8. Line removal demonstration with the single-detector version of SEECR. The bottom sub-panel shows the time series of the signal and the top sub-panel shows the periodogram of the data before and after removing the SEECR estimate of the signal. (The frequency resolution here is 0.5 Hz.) The red curve in the bottom sub-panel shows the estimated amplitude envelope of the signal.

lower signal SNRs than typically presented by the lines in real data, it offers the potential of substantially improving the estimate.

A. Single line

Fig. 8 demonstrates SEECR as a line remover. A 1.5 sec long amplitude modulated sinusoid, with an SNR that is much weaker than those of typical lines in real data, is estimated using SEECR. Subtracting this estimate is seen to get rid of the line almost completely. More importantly, unlike the LPF, the subtraction does not leave behind a noticeable notch. Note that, besides the instantaneous frequency, the amplitude envelope of a line must also be estimated for its subtraction to be effective.

B. Multiple lines

One of the main issues in line removal for a method such as SEECR, which assumes that there is only a single chirp in the data, is the presence of multiple lines. The simplest strategy in this case is to run SEECR with the search range in instantaneous frequency values ($\overline{\nu}$ in Sec. 1) restricted to some band around each line. Thus, if there are lines in the data with carrier frequencies f_i, $i = 1, 2, \ldots, P$ in ascending order, we run SEECR independently P times with search ranges $|v_k - f_i| \leq l_i \leq \min(f_{i+1} - f_i, f_i - f_{i-1})$, $k = 1, 2, \ldots, K$. Each run of SEECR produces an estimate of the respective line that can then be subtracted from the data.

Fig. 9 shows the effectiveness of this strategy for different separations between the frequencies of two monochromatic signals in white noise. The frequency of one line is fixed at $f_1 = 250$ Hz and that of the other, f_2, is varied. Only the line at f_1 is estimated and removed. The search range for instantaneous frequency values in SEECR is kept fixed at $l_1 = 50$ Hz.

The simple strategy above is observed to work well when the two lines have equal SNR: E_{res} is reduced to 4% of E_{data}

ISBN 978-90-827970-1-5 © EURASIP 2018

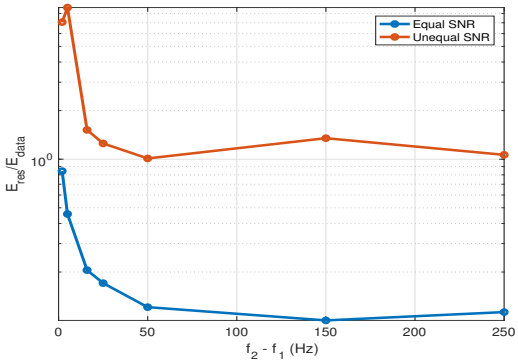

Fig. 9. Removal of a monochromatic line at frequency $f_1 = 250$ Hz in the presence of a second line at frequency f_2. The quantity E_A is the average periodogram of a sequence A over the range $f_1 \pm 1$ Hz. $A =$ 'data' and 'res' respectively denote the data and the residual obtained from it after subtracting out the estimated signal. The two curves correspond to the two lines having (blue) equal and (orange) unequal amplitudes. In the latter case, the amplitude of the line at f_2 is a factor of 100 higher than that of the line at f_1.

in the immediate neighborhood of f_1 even when $l_1 = f_2 - f_1$. Since the assumption of a single chirp becomes progressively worse with decreasing $f_2 - f_1$, the effectiveness of the strategy is reduced when the two lines move closer to each other. In contrast, the strategy is a total failure if the line that is not being removed (i.e. f_2) is much stronger.

V. Conclusions

SEECR is found to be an effective method for detecting and estimating transient chirps. In particular, it improves the detectability of unmodeled GW chirps at signal strengths where time-frequency clustering, the basis of the principal GW burst search methods, is seen to fail.

We presented a first application of SEECR to the case of non-transient chirp estimation and subtraction, a problem that is highly relevant to GW data analysis given the presence of high power line interference. While SEECR performs quite well when the data has a single line or multiple lines with comparable strengths, simple strategies to extend its application to the case of highly disparate strengths do not suffice. It is possible that evaluating the fitness function in the frequency rather than time domain, with a restriction on the range of frequencies used, can lead to a significant improvement in performance. This and other ideas will need to be explored in future work.

Acknowledgment

This work was supported by National Science Foundation Grant No. PHY-1505861. We acknowledge the Texas Advanced Computing Center (TACC) at The University of Texas at Austin for providing HPC resources that have contributed to the research results reported within this paper. URL: http://www.tacc.utexas.edu

References

[1] P. Fritschel, "Second generation instruments for the Laser Interferometer Gravitational Wave Observatory (LIGO)," in *Gravitational-Wave Detection*, ser. Society of Photo-Optical Instrumentation Engineers (SPIE) Conference Series, M. Cruise and P. Saulson, Eds., vol. 4856, Mar. 2003, pp. 282–291.

[2] J. Degallaix, T. Accadia, F. Acernese, M. Agathos, A. Allocca *et al.*, "Advanced Virgo Status," in *9th LISA Symposium*, ser. Astronomical Society of the Pacific Conference Series, G. Auger, P. Binétruy, and E. Plagnol, Eds., vol. 467, Jan. 2013, p. 151.

[3] LIGO Scientific Collaboration. Detection of gravitational waves. [Online]. Available: https://www.ligo.org/detections.php

[4] C. W. Helstrom, *Statistical Theory of Signal Detection*. Pergamon, London, 1968.

[5] S. D. Mohanty, "Spline based search method for unmodeled transient gravitational wave chirps," *Phys. Rev. D*, vol. 96, p. 102008, Nov 2017.

[6] S. Klimenko *et al.*, "Method for detection and reconstruction of gravitational wave transients with networks of advanced detectors," *Phys. Rev. D*, vol. 93, p. 042004, Feb 2016.

[7] N. J. Cornish and T. B. Littenberg, "Bayeswave: Bayesian inference for gravitational wave bursts and instrument glitches," *Classical and Quantum Gravity*, vol. 32, no. 13, p. 135012, 2015.

[8] R. Lynch, S. Vitale, R. Essick, E. Katsavounidis, and F. Robinet, "Information-theoretic approach to the gravitational-wave burst detection problem," *Phys. Rev. D*, vol. 95, no. 10, p. 104046, May 2017.

[9] P. J. Sutton, G. Jones, S. Chatterji, P. Kalmus, I. Leonor, S. Poprocki, J. Rollins, A. Searle, L. Stein, M. Tinto, and M. Was, "X-Pipeline: an analysis package for autonomous gravitational-wave burst searches," *New Journal of Physics*, vol. 12, p. 053034, 2010.

[10] S. D. Mohanty, "Particle swarm optimization and regression analysis II," *Astronomical Review*, vol. 7, no. 4, pp. 4–25, 2012.

[11] R. Eberhart and J. Kennedy, "A new optimizer using particle swarm theory," in *Micro Machine and Human Science, 1995. MHS'95., Proceedings of the Sixth International Symposium on*. IEEE, 1995, pp. 39–43.

[12] C. de Boor, *A Practical Guide to Splines (Applied Mathematical Sciences)*. Springer, 2001.

[13] D. Ruppert, M. P. Wand, and R. J. Carroll, *Semiparametric regression*. Cambridge University Press, 2003.

[14] D. Fraser and H. Massam, "A mixed primal-dual bases algorithm for regression under inequality constraints. application to concave regression," *Scandinavian Journal of Statistics*, vol. 16, pp. 65–74, 1989.

[15] G. H. Golub, M. Heath, and G. Wahba, "Generalized cross-validation as a method for choosing a good ridge parameter," *Technometrics*, vol. 21, no. 2, pp. 215–223, 1979.

[16] C. Leung, "Estimation of unmodeled gravitational wave transients with spline regression and particle swarm optimization," *SIAM Undergraduate Research Online (SIURO)*, vol. 8, 2015.

[17] H. Akaike, "Information theory and an extension of the maximum likelihood principle," in *Selected Papers of Hirotugu Akaike*. Springer, 1998, pp. 199–213.

[18] D. Bratton and J. Kennedy, "Defining a standard for particle swarm optimization," in *Swarm Intelligence Symposium, 2007. SIS 2007. IEEE*. IEEE, 2007, pp. 120–127.

[19] Y. Wang, S. D. Mohanty, and F. A. Jenet, "Coherent Network Analysis for Continuous Gravitational Wave Signals in a Pulsar Timing Array: Pulsar Phases as Extrinsic Parameters," *Astrophy. J.*, vol. 815, p. 125, Dec. 2015.

[20] S. S. Haykin, *Adaptive filter theory*. Pearson Education India, 2008.

[21] S. Chatterji, L. Blackburn, G. Martin, and E. Katsavounidis, "Multiresolution techniques for the detection of gravitational-wave bursts," *Classical and Quantum Gravity*, vol. 21, no. 20, p. S1809, 2004.

[22] MATLAB, *version 9.0 (R2016a)*. Natick, Massachusetts: The MathWorks Inc., 2016.

[23] B. P. Abbott *et al.*, "Observation of gravitational waves from a binary black hole merger," *Phys. Rev. Lett.*, vol. 116, p. 061102, Feb 2016.

[24] W. Hardle, "Applied nonparametric regression," *Econometric Society Monographs*, vol. 19, 1990, cambridge University Press.

[25] S. D. Mohanty, "Median based line tracker (MBLT): model independent and transient preserving line removal from interferometric data," *Classical and Quantum Gravity*, vol. 19, pp. 1513–1519, Apr. 2002.

ISBN 978-90-827970-1-5 © EURASIP 2018